

Estimation of Operative Line of Resection Using Preoperative Image and Nonrigid Registration

Jong-Ha Lee, Chang-Hee Won, and Seong-Gon Kong

Abstract—Even though accurate diagnosis of organs is done using preoperative images such as CT or MRI, these information are not directly used in the operating room, because organs are nonrigid and their shapes change with time. In this paper, we propose to obtain an intraoperative image of an open organ and fuse the image with a preoperative image. The intraoperative image is obtained from a three-dimensional laser scanner. The registration of preoperative image to the intraoperative image can relate the information from the preoperative image to the open organ in the operating room. We do this by registering preoperative images to intraoperative images. An algorithm based on Robust Point Matching method is developed for this nonrigid image registration problem. We also propose a new metric called Non Overlapping Ratio to determine the registration error. The experiments demonstrate that the proposed method is capable of achieving region of interest estimation within 1.51 mm mean distance error and 0.66% Non Overlapping Ratio.

I. INTRODUCTION

The anatomical locations of unhealthy tissues can be determined preoperatively using imaging modalities such as Computer Tomography (CT), Single Photon Emission Computerized Tomography (SPECT), and Magnetic Resonance Imaging (MRI). These systems assist surgeons to locate the target and plan an operative process. However, tissue deformation during the surgery makes it difficult to locate diseased region accurately. Acquiring intraoperative images in the Operating Room (OR) and registering with preoperative data can help overcome the difficulties created by the lack of correspondences.

One method of generating intraoperative images is to use high-resolution three-dimensional laser scanner [1], [2]. The laser scanner acquires a dense surface data and creates three-dimensional point clouds. This method has several advantages compared to other intraoperative imaging acquisition methods. Since it is based on the optical measurement, the scanner can circumvent problems of radiation exposure from CT, and metallic surgery tool effect associated with MRI. In addition, avoiding direct contact with patients eliminate possible errors from tissue deformation, often caused in the ultrasound probing method. The laser scanner has been successfully used in the brain and the liver cortical surface tracking problems [3], [4].

This work was supported by the Office of the Senior Vice President for Research and Strategic Initiatives at Temple University

Jong-Ha Lee is with the Department of Electrical and Computer Engineering, Temple University, PA 19122, USA

Chang-Hee Won is an assistant professor in the Department of Electrical and Computer Engineering, Temple University, PA 19122, USA

Seong-Gon Kong is an associate professor in the Department of Electrical and Computer Engineering, Temple University, PA 19122, USA

The objective of this study is to develop a method to obtain the preoperative Region of Interest (ROI) using intraoperative laser scanner images, and nonrigid image registration for the surgeons. Our method starts from the landmarks identification. Landmarks on images are identified along the visible anatomy by surgeons in the OR. Because the laser scanner detects ridgelines of an object instead of the color, surgeons may not determine some anatomical boundaries with laser scanner images. Thus, we segment the CT image landmarks into CT outline landmarks and CT ROI landmarks. ROI is the region where surgeons intend to resect but unable to differentiate within laser scanner images.

In the paper of [5], Thin Plate Spline (TPS) and Robust Point Matching (RPM) have been developed specifically for nonrigid image registration. The TPS-RPM algorithm uses continuous relaxations for correspondence variables and Thin Plate Spline for nonrigid mapping. In this paper, TPS affine transformation and non-affine deformation matrices are found while registering CT outline landmarks and laser scanner landmarks by RPM. Then these two matrices are applied to CT ROI landmarks and estimates the transformed ROI landmarks without correspondence; this part is a novel addition to the algorithm described in [5]. Finally, estimated ROI landmarks are overlaid onto laser scanner landmarks and surgeons identifies their ROI intraoperatively. Previous efforts have been made to characterize lesion position by radio-opaque metal clips, Tc-99m labeled Nanocol or tattoos to overcome intraoperative tissue deformation [6], [7], [8]. The operative ROI estimation method can be applied to most nonrigid organ surgery for intraoperative guidance.

In the remainder of the paper, we first describe the system to acquire images preoperatively and intraoperatively in Section II-A and B. We then review TPS-RPM algorithm briefly and present our ROI estimation method in Section II-C. A new metric for registration accuracy is introduced in Section II-D and used in Section III. Finally, conclusions are given in Section IV.

II. MATERIALS AND METHODS

A. CT Images Acquisition

Preoperative imaging from various different modalities is usable with our method. In this paper, we obtained 3D CT images of a pig's lung from a 64 multi slice high resolution Siemens Somatom Sensation CT scanner in Temple University Hospital. The CT produced multiple 2D slices with 0.24 mm resolution with scanning time less than 30 seconds. Then we used the software from Siemens to generate 3D CT images. The images were stored in a format Dicom (Digital

TABLE I

SWINE LUNG SCANNING TEST WITH OPTIX 400M LASER SCANNER

| Lines | Points | Resolution X(mm) | Resolution Y(mm) | Time(s) |
|-------|--------|------------------|------------------|---------|
| 1000 | 1000 | 0.25 | 0.25 | 90 |
| 500 | 1000 | 0.40 | 0.25 | 75 |
| 300 | 1000 | 0.75 | 0.25 | 50 |
| 500 | 255 | 0.40 | 0.75 | 20 |

Imaging and Communication in Medicine). The number of Dicom files collected from the CT depends on how thin the 2D slices were chosen.

B. Laser Scanner Images Acquisition

We used a laser scanner (Optix 400M, 3D Digital Corporation, Sandy Hook, CT) to obtain intraoperative images. The resolution was 0.175 mm at 30 cm range (0.007 inches at 12 inches away) and 0.375 mm at 65 cm range (0.015 inches at 26 inches away). The point density was 1,000 points per stripe, up to 1,000 lines, and the field of view was 30 degrees. If the object is glossy or light absorbing such as black in color, then the scanned image may be noisy or the sensor may not detect the laser light reflection. We have tested this hypothesis through an experiment with a pig's lung. A pig's lung was pinkish in color with a smooth, light, porous, spongy texture, and the scanner was able to scan it. We also have experimented with the point density, resolution, and scanning time. The results are summarized in Table I. The preliminary result shows that the best resolution of X and Y was 0.25 mm with 90 seconds scanning time and the worst resolution was 0.40 mm of X and 0.75 mm of Y with 20 seconds scanning time. The organ such as a lung is not stationary for 90 seconds. However, the surgeons can inflate one lung at a time and hold it at a constant pressure for 90 seconds. Then we can scan to lung during this period. In the OR, there is a need to relate the laser scanner space with a fixed coordinate system. To relate laser scanner images to the physical space and track the laser scanner accurately, we designed the system to use a Coordinate Measurement Machine (CMM), a device for dimensional measuring and it obtains the coordinates of points on an object surface.

C. Preoperative Anatomical Boundary Estimation

Suppose we have a preoperative CT image and an intraoperative laser scanner image. The point set matrix $X = \{x_i : i = 1, \dots, l\}$ is sampled along the outline of an object on CT images and the point set matrix $Y = \{y_j : j = 1, \dots, m\}$ is sampled along the ROI of an object on CT images. The point set matrix $Z = \{z_k : k = 1, \dots, n\}$ is sampled from an object on laser scanner images. Since the scanner cannot detect the ROI, the corresponding points of the ROI on CT images does not exist. Our task is to find this intraoperative ROI without corresponding points from the preoperative image. We propose to register X to Z by nonrigid registration method and finds affine transformation and non-affine transformation. These two matrices are then applied to Y to transform along the previously found warp field. The nonrigid registration

method we use is based on TPS-RPM algorithm [5]. TPS-RPM algorithm uses softassign, deterministic annealing, and TPS for the spatial mapping and the outlier rejection to solve for both correspondences and mapping parameters. The TPS fits a mapping function by minimizing following energy functions:

$$E(f) = \sum_{i=1}^l \left\| \hat{Z} - f(x_i) \right\|^2 + \lambda \int \int \left[\left(\frac{\partial^2 f}{\partial x^2} \right)^2 + 2 \left(\frac{\partial^2 f}{\partial x \partial y} \right)^2 + \left(\frac{\partial^2 f}{\partial y^2} \right)^2 \right] dx dy \quad (1)$$

The point set matrix $\hat{Z} = \{z_k : k = 1, \dots, n\}$ is newly estimated positions that corresponds to X . With a fixed weight parameter λ , a unique solution that minimizes $E(f)$ exists. The solution consists of two matrices A and B as

$$f(x_i, A, B) = x_i \cdot A + \phi(x_i) \cdot B \quad (2)$$

where A is a 3×3 matrix representing the affine transformation and B is a $l \times 3$ warping coefficient matrix representing the non-affine deformation. $\phi(x_i)$ is a $1 \times l$ vector with each entry $\phi_j(x_i) = \|x_j - x_i\|^2 \log \|x_j - x_i\|$, $i, j = 1, \dots, l$ [9]. All $\phi_j(x_i)$ stack together and comprise the TPS kernel ϕ . If we substitute the solution for (2) into (1), the actual TPS energy function in TPS-RPM algorithm becomes,

$$E(f) = \left\| \hat{Z} - XA - \Psi B \right\|^2 + \lambda_1 \text{trace}(A^T \Psi B) + \lambda_2 \text{trace}|A - I|^T |A - I| \quad (3)$$

where $\lambda_1 = \lambda_1^{init} T$, $\lambda_2 = \lambda_2^{init} T$, and $T_{new} = T_{old} \tau$ with $\lambda_1, \lambda_2, T, \tau \in [0, 1]$. $\Psi = \{\phi(x_i) : i = 1, \dots, l\}$ is a $l \times l$ matrix. The parameters λ_1 and λ_2 are weighting parameters and T is the searching scope of X . To find least-squares solutions for A and B , we apply QR decomposition on X to separate the affine and non-affine warping space [10].

$$X = [Q_1 | Q_2] \begin{pmatrix} R \\ 0 \end{pmatrix} \quad (4)$$

The final optimal solutions for A and B we obtain as

$$A = R^{-1} (Q_1^T \hat{Z} - \Psi B) \quad (5)$$

$$B = Q_2 (Q_2^T \Psi Q_2 + \lambda I)^{-1} Q_2^T \hat{Z} \quad (6)$$

The affine transformation matrix A and non-affine deformation matrix B makes a smooth warp field that maps CT images onto laser scanner images. TPS-RPM algorithm estimates A and B while gradually reduce T and the algorithm stops when T reaches T_{final} . Since we know the transformation A and B in every determined annealing step, we can gradually transform CT ROI point set Y together without corresponding points.

| The Operative ROI Estimation Algorithm Pseudo-code |
|---|
| Input: X, Y, Z |
| Initialization: $A \leftarrow 0, B \leftarrow 0, T \leftarrow T_o, \lambda \leftarrow \lambda_o$ |
| Do 1: Deterministic Annealing between X and Z |
| Do 2: Alternating Update |
| Update correspondence based on current A and B |
| Update A and B based on current correspondence |
| Update \hat{Y} based on updated A and B |
| Until 2 A and B are converged |
| End Alternating Update |
| $T \leftarrow T\tau, \lambda \leftarrow \lambda T$ |
| Until 1 $T < T_{final}$ |
| Merge \hat{Y} and \hat{Z} |
| End Deterministic Annealing |

D. Performance Metrics of Registration Accuracy

The measurement of Root Mean Square (RMS) between corresponding points after registration is the most common performance metric of registration accuracy in rigid landmarks based registration. If landmarks are used for calculating the registration, it is Fiducial Registration Error (FRE). If not, it is Target Registration Error (TRE). The closest corresponding metric to FRE and TRE for non rigid registration is measuring mean RMS distance error (MRE) between points on one image and its corresponding closest points on the other image [4]. However this metric is inconsistent and sometimes leads to misleading results. Figure 2 shows the failure of MRE for the registration accuracy in the non rigid registration. As can be seen, poor registration on the right may appear to be the same error with the good registration on the left. In order to overcome this drawback

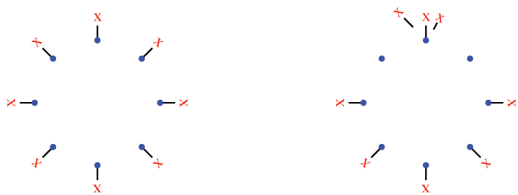


Fig. 1. An example of the failure of MRE for the registration accuracy in the non rigid registration. Good registration result on the left and poor registration result on the right has a similar MRE.

of MRE, we introduce a new metric called Non Overlapping Ratio (NOR). Our main concern is the mismatched area after registration. If image A is registered to image B , then NOR gives

$$NOR = \frac{R(A \cup B) - 2R(A \cap B)}{R(B)} \times 100(\%) \quad (7)$$

$R(\cdot)$ indicates the area approximated by a polygon of landmarks. This value will be zero if there is no overlapping and 100 % if images are matched perfectly. Using NOR gives more intuitive metric of the mismatched area.

III. EXPERIMENT AND RESULTS

All experiment results in this paper used 220 landmarks ($i = 200, j = 20, k = 220$). Two different models and image sources are considered in this paper.

TABLE II
REGISTRATION RESULTS OF DIGITAL IMAGE

| Trial | Outline | | Region of Interest | |
|-------|----------|---------|--------------------|---------|
| | MRE (mm) | NOR (%) | MRE (mm) | NOR (%) |
| 1 | 1.39 | 0.62 | 1.65 | 0.69 |
| 2 | 1.21 | 0.67 | 1.42 | 0.63 |
| 3 | 1.58 | 0.72 | 1.54 | 0.64 |
| 4 | 1.30 | 0.56 | 1.21 | 0.57 |
| 5 | 1.23 | 0.54 | 1.43 | 0.60 |
| 6 | 1.42 | 0.55 | 1.45 | 0.62 |
| 7 | 1.27 | 0.49 | 1.41 | 0.60 |
| 8 | 0.85 | 0.45 | 1.54 | 0.68 |
| 9 | 0.99 | 0.53 | 1.49 | 0.74 |
| 10 | 1.28 | 0.52 | 1.97 | 0.82 |
| mean | 1.25 | 0.57 | 1.51 | 0.66 |

- 1) Case 1: Balloon digital images, ROI is visible on both images
- 2) Case 2: Pig lung CT image / laser scanner image, ROI is shown on the CT image but not on the laser scanner image.

Our method can be applicable to most nonrigid organs. In case 1, we used balloons to simulate human's organ. Before taking a picture, we drew a line on the balloon's surface to indicate a truth line of ROI. We took the first digital image with inflated balloon (221 mm (h) x 168 mm (v)) and took the second image with deflated balloon (178 mm (h) x 123 mm (v)). In case 2, we used a commercial pig's lung, another nonrigid model. The inflated pig lung (321 mm (h) x 374 mm (v)) was scanned by a CT and the deflated pig's lung (282 mm (h) x 358 mm (v)) was scanned by a laser scanner. To increase the reliability of the experiment, we made 10 different landmarks point sets and calculated the statistical characteristics of registration results. The computer used for the experiments was a 64 bit Windows machine with 3GHz processor and 2GB memory. The running time was less than one minute for 220 landmarks.

A. Case 1: Balloon Digital Images

Experiment results show that in case 1, ROI landmarks registration without corresponding points is very close to outline landmarks registration with corresponding points. Table II summarizes the results. The resulting mean value of MRE was 1.51 mm and NOR was 0.66% for ROI landmarks compare to 1.25 mm MRE and 0.57% NOR for outline landmarks. Note that in fourth trial of ROI landmarks, MRE and NOR was 13% and 8% lower than that of first trial of outline landmarks. It means that the registration result depends on the landmark point sets. If we carefully choose the landmarks, then we can decrease the amount of ROI estimation error

We also notice that NOR of third trial of ROI landmarks was 5% lower than that of eighth trial of ROI landmarks even though MRE was the same. From this information, we note that the registration result on third trial is better than that of eighth one. It indicates that a new metric NOR can be a good measure of the registration accuracy, and compensates the drawbacks of the MRE.

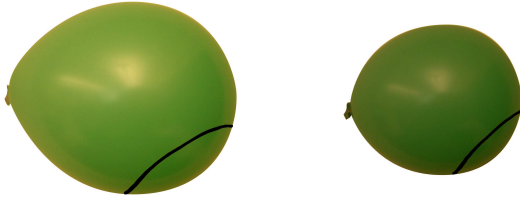


Fig. 2. Digital image of the inflated balloon with ROI ground truth (left) and deflated balloon with ROI ground truth (right).

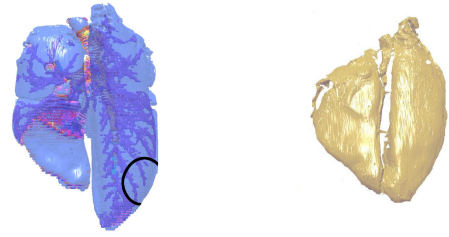


Fig. 4. CT image of inflated pig's lung with ROI ground truth (left) and laser scanner image of deflated pig's lung without ROI ground truth (right).

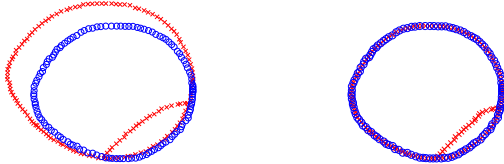


Fig. 3. The landmarks point sets before registration (left) and after registration using ROI estimation method (right) in digital images experiment.



Fig. 5. The landmarks point sets before registration (left) and after registration using ROI estimation method (right) in CT image / Laser Scanner image experiment.

B. Case 2: Pig's Lung CT Image / Laser scanner Image

Because there are no truth lines of ROI on laser scanner images, we show only outline landmarks result in Table III. The resulting mean value of MRE was 2.43 mm and NOR was 1.40% for outline landmarks, 49% and 59% higher than the case 1 outline landmarks. This is because the pig's lung model is the higher degree of deformation than the balloon. Similar to the case 1, we notice that NOR is a good metric for the registration accuracy. We note that the tenth trial NOR is better than the fifth trial even MRE is the same. This shows NOR is a more intuitive measure of the registration error.

IV. CONCLUSIONS

We proposed the estimation method to find the operative ROI from the peroperative images without corresponding points. For this, we used CT images as the preoperative images, laser scanner images as the intraoperative images, and TPS-RPM based algorithm for non-rigid image registration. To quantify the registration error intuitively, we proposed

Non Overlapping Ratio. Our results show that operative ROI estimation without corresponding points method is relatively fast and convenient for the OR environment, and offers a tool to support the surgeon's resection boundary decision.

REFERENCES

- [1] M. Botsch, B. Chen, "Laser Scanner Super-resolution", *Eurographics Symposium on Point-Based Graphics*, 2006.
- [2] T. Sohmlura, M. Nagao, M. Sakai, K. Wakabayashi, T. Kojima, S. Kituta, T. Nakamura, and J. Takahashi, "High-Resolution 3-D Shape Integration of Dentition and Face Measured by New Laser Scanner", *IEEE Transactions on Medical Imaging*, vol. 23, num. 5, pp. 633-638, 2004.
- [3] S. Ding, M. Miga, R. R. Tompson, P. Dumpuri, A. Cao, and B. Dawant, "Estimation of Intra-Operative Brain Shift using a Tracked Laser Range Scanner", *IEEE International Conference of EMBS*, pp. 848-851, 2007.
- [4] D. Cash, T. Sinha, W. Chapman, H. Terawaki, B. Dawant, R. Galloway, and M. Miga, "Incorporation of a Laser Range Scanner into Image-Guided Liver Surgery: Surface Acquisition, Registration, and Tracking", *Journals of Medical Physics*, pp. 1671-1682, 2003.
- [5] H. Chui, J. Rambe, R. Schultz, and A. Rangaraian, "Registration of Cortical Anatomical Structures via Robust 3D Point Matching", *In Processing in Medical Imaging*, pp. 168-181, 1999.
- [6] T. Deliiski, S. Popovska, and D. Dardanov, "A Method for Marking the Location of Breast Cancer Tumor Indicated for Neo-Adjuvant Chemotherapy", *Journal of International Medical Association, Bulgaria*, 2004.
- [7] M. Lassanen, J. Heikkinen, S. Sarrakkala, and H. Paajanen, "Localization of Sentinel Nodes in Breast Cancer: Novel Method and Device to Help Pen Marking of Active Nodes during Gamma Camera Imaging", *Journal of Physics in Medicine and Biology*, 2005.
- [8] D. Lannin, B. Grube, S. Black, and T. Ponn, "Breast Tattoos for Planning Surgery following Neoadjuvant Chemotherapy", *American Journal of Surgery*, 2007.
- [9] G. Wahba, "Spline Models for Observational Data", *Series in Applied Mathematics*, vol. 59, 1990.
- [10] H. Chui, and A. Rangaraian, "A New Algorithm for Non-rigid Point Matching", *In Processing of IEEE Conference on Computer Vision and Pattern Recognition*, vol. 2, pp. 44-51, 2000.

TABLE III
REGISTRATION RESULTS OF CT IMAGE / LASER SCANNER IMAGE

| Trial | Outline | |
|-------|----------|---------|
| | MRE (mm) | NOR (%) |
| 1 | 2.24 | 1.34 |
| 2 | 2.37 | 1.42 |
| 3 | 2.48 | 1.46 |
| 4 | 2.72 | 1.57 |
| 5 | 2.42 | 1.34 |
| 6 | 2.34 | 1.47 |
| 7 | 2.76 | 1.58 |
| 8 | 2.30 | 1.48 |
| 9 | 2.23 | 1.20 |
| 10 | 2.42 | 1.17 |
| mean | 2.43 | 1.40 |